iScience

CellPress
OPEN ACCESS

Article

Ion permeation controlled by hydrophobic residues and proton binding in the proton-activated chloride channel

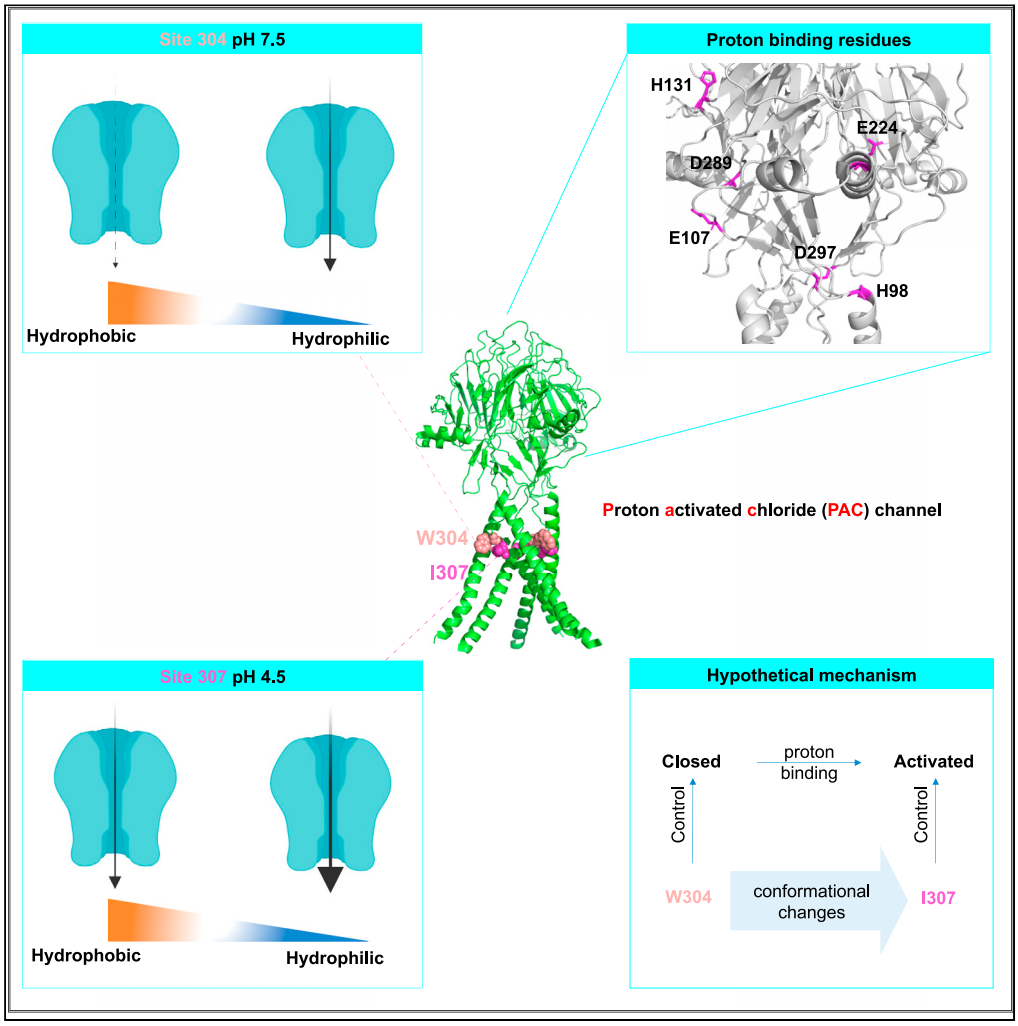

Ruiqi Cai, Jingfeng Tang, Xing-Zhen Chen

xzchen@ualberta.ca (X.-Z.C.)
tangjingfeng@hbut.edu.cn (J.T.)

Highlights

The hydrophobicity of site 304 is critical for maintaining PAC at a closed state

The function of activated PAC is modulated by the hydrophilicity of site 307

Six protonatable amino acids are involved in proton-induced PAC activation

H^+ binding seem to change PAC from W304-controlled closed to I307-gated open state

Cai et al., iScience 24, 103395
December 17, 2021
https://doi.org/10.1016/j.isci.2021.103395

iScience

CellPress
OPEN ACCESS

Article

Ion permeation controlled by hydrophobic residues and proton binding in the proton-activated chloride channel

Ruiqi Cai,[1] Jingfeng Tang,[2,*] and Xing-Zhen Chen[1,3,*]

SUMMARY

Recently identified proton-activated chloride channel (PAC) contains two transmembrane helices (S1–S2) and is involved in lysosome function, hypoxia adaption, stroke, and carcinogenesis. Although a PAC structure was recently resolved, its gating and activation mechanisms remained largely unknown. By the two-electrode voltage clamp electrophysiology in *Xenopus* oocytes, we found that the hydrophobicity of site 304 at fenestrations, but not that of neighbor sites, is important for maintaining PAC at a closed state at pH 7.5. When activated at acidic pH, PAC activity significantly increased with the hydrophilicity of site 307 within S2, but not with that of neighbor sites, suggesting that 307 acts as an activation gate. We identified six conserved protonatable residues critical for proton-induced activation, consistent with structural studies. Our study depicted a scheme in which proton binding induces conformational changes from the W304-controlled closed state at fenestrations to an activated state controlled by activation gate I307 in helix S2.

INTRODUCTION

As the most prevalent extracellular anion, chloride (Cl) ion passes biological membranes via Cl transporters or channels, previously classified into six families without apparent sequence homology to each other: anoctamins, bestrophins, ligand-gated anion channels, cAMP-activated Cl channels, volume-regulated anion channels, and voltage-gated ClC channels (Duran et al., 2010; Terry, 1994). Cl channels play key roles in cell volume regulation, electrical excitability, transepithelial transport, and ion homeostasis. Thus, abnormal function of Cl channels may result in channelopathies that include hyperekplexia, epilepsy, osteopetrosis, lysosome storage disorder, neurodegeneration, and cystic fibrosis (Planells-Cases and Jentsch, 2009). A Cl channel with acid-induced outward rectification and with characteristics distinct from the known Cl channels remains to be molecularly identified although several previous studies described it in cultured human embryonic kidney (HEK) cells, sertoli cells, umbilical vein endothelia, hippocampal, and cardiac myocytes (Auzanneau et al., 2003; Capurro et al., 2015; Lambert and Oberwinkler, 2005; Ma et al., 2008; Yamamoto and Ehara, 2006). Previously undetermined membrane protein TMEM206 was recently characterized as a proton-activated Cl channel (PAC) through RNA interference screen (Ullrich et al., 2019; Yang et al., 2019). Enriched expression of *PAC* in human tissues has been found in cerebral cortex, lymph node, bone marrow, spleen, kidney, lung, and bladder via RNA sequencing (Yang et al., 2019). PAC is activated by low extracellular pH, inducing cell death along with Cl^- influx (Yang et al., 2019). Temperature is known to enhance the sensitivity of PAC to protons, with an unclear mechanism (Sato-Numata et al., 2014). Under pathological conditions such as stroke and ischemia-reperfusion and acidic environments, PAC may be involved in neuronal cell death. PAC knockout in mice protects brain ischemia-reperfusion caused neuronal death (Yang et al., 2019). As for cell microenvironment, pericellular-acidic pH promotes cancer cell migration and invasion, while acidosis impairs immunological functions and is associated with immunodeficiency (Lardner, 2001). Of note, genomic sequencing in both Tibetans and Tibetan swine revealed that *PAC* genomic region exhibits one of the strongest increases in the allele frequencies, suggesting an underlying role of PAC in adaption to hypoxia (Dong et al., 2014; Yi et al., 2010).

PAC is predicted to contain two hydrophobic membrane-spanning segments (S1 and S2), a large extracellular loop as well as the cytosolic N- and C-termini (Ullrich et al., 2019). Using cysteine mutation scanning, the second transmembrane helix S2 (N302-F318 in human PAC) was suggested as a pore-forming domain

[1]Department of Physiology, Faculty of Medicine and Dentistry, University of Alberta, Edmonton, AB T6G 2H7, Canada

[2]National "111" Center for Cellular Regulation and Molecular Pharmaceutics, Hubei University of Technology, Wuhan, Hubei 430086, China

[3]Lead contact

*Correspondence: xzchen@ualberta.ca (X.-Z.C.), tangjingfeng@hbut.edu.cn (J.T.)

https://doi.org/10.1016/j.isci.2021.103395

(Ullrich et al., 2019; Yang et al., 2019). Given no sequence similarity to any known channels and limited knowledge on the function, the regulation and gating mechanism of PAC have yet to be investigated. We recently documented a hydrophobic gate mechanism in seven members within the transient receptor potential (TRP) superfamily of cation channels that adopt a single- or double-consecutive-residue gate (Zheng et al., 2018b, 2018c) in the pore-lining S6 helix. According to the hydrophobic gate theory, a pore composed of an hydrophobic amino acid(s) forms an energetic barrier that allows effective control of ion permeation (Aryal et al., 2015), which have been validated in numerous channels by structural, electrophysiological, or molecular dynamic (MD) studies (Aryal et al., 2015). Cryogenic electron microscopy (cryo-EM) structures of human and pufferfish PAC have recently become available from two groups (Deng et al., 2021; Ruan et al., 2020). Note that these structures were captured at non-conducting configurations. Several constrictions were present at the proposed lateral fenestrations and ion permeation pathway. The functional role of the fenestrations and the pore gate within the ion permeation pathway remain to be characterized.

Prior to the molecular identification of PAC, proton-induced Cl currents have been extensively documented and linked to acidosis-related cell death in cultured neuronal, cardiac, epithelial, and blood cells (Valinsky et al., 2017; Wang et al., 2007; Yamamoto and Ehara, 2006). The half-maximum activation is around pH 5.0 with a best-fit Hill coefficient of 3.6, suggesting that more than one proton ion cooperatively binds to activate PAC (Lambert and Oberwinkler, 2005). The newly discovered PAC protein sequence allows the examination of the proton binding sites. Insensitivity of the PAC outward rectifying current to intracellular pH buffering suggests that the residues involved in proton binding are located in the extracellular loop.

In the present study, we examined the functional importance of residues around the lateral fenestrations and putative pore gate and those potentially involved in proton binding by means of electrophysiology with *Xenopus* oocytes, in combination with molecular biology and immunofluorescence. By flow cytometry, we also examined the effect of a gain-of-function (GOF) mutant PAC on the death of HEK 293 cells and a widely used neuronal cell model human SH-SYSY cells.

RESULTS

Identification of residues in proton-activated chloride channel that control ion flow

PAC is closed at extracellular pH 7.5 and is fully activated when pH decreases to around 4.5 (Yang et al., 2019). PAC structures revealed that W304 and nearby residues form lateral fenestration tunnels that were predicted to control Cl flow by MD simulations (Ruan et al., 2020). Based on a hydrophobic gate theory, a hydrophobic, but not hydrophilic, residue from each PAC subunit may together form an energy barrier that allows controlling of the flow of hydrated ions, that is, acting as a gate residue (Aryal et al., 2015). Replacing a hydrophobic gate residue with a hydrophilic or less hydrophobic residue should abolish the hydrophobic barrier and constitutively open the pore at extracellular pH 7.5 (Aryal et al., 2015). Based on this theory, we here examined PAC hydrophobic residue(s) within helix S2 (Figure 1A) that would result in increased Cl flow upon hydrophilic substitutions. For this, each of the 11 hydrophobic residues between W304 and F318 in the putative pore-lining S2 helix (Yang et al., 2019) was individually mutated to hydrophilic asparagine (N) and the function of the resulting mutant channels studied using *Xenopus* oocyte expression together with the two-electrode voltage clamp. Eight out of the eleven hydrophobic residues are highly conserved across different species (Figure 1A). By biotinylation, Western blotting and immunofluorescence assays we found that the surface expression of these mutants is similar to that of wild-type (WT) channel (Figure S1). Mutant channel W304N, but not the WT or any other mutant channels, exhibited substantially increased channel activity at extracellular pH 7.5 (Figures 1B and 1C). Interestingly, unlike WT PAC, the activity of mutant W304N only slightly increased when pH dropped from 7.5 to 4.5 (Figure 1D). Because of outward rectification of PAC, we also utilized currents at +80 mV as a function readout, as previously employed (Ullrich et al., 2019; Yang et al., 2019). At +80 mV, the W304N mutant activity remained unaffected when changing from pH 7.5 to pH 4.5, that is, substitution with hydrophilic N resulted in increased channel activity equivalent to proton-activated WT PAC activity (Figure 1E). Thus, W304 is critical in maintaining PAC at a closed state at pH 7.5. However, based on PAC structures, W304 is not part of the central pore formed by helix S2 but is rather at lateral fenestrations and seems to point to the ion-conducting pathway at fenestrations (Ruan et al., 2020). To further emphasize the functional importance of W304, we examined the roles of two adjacent hydrophobic residues I298 and I299 in pre-S2 are at fenestrations (Ruan et al., 2020). We found that substitution with N or A at either site has no effect on the function (Figure S2). Together, these data indicated that conserved hydrophobic residue W304 at fenestrations, but

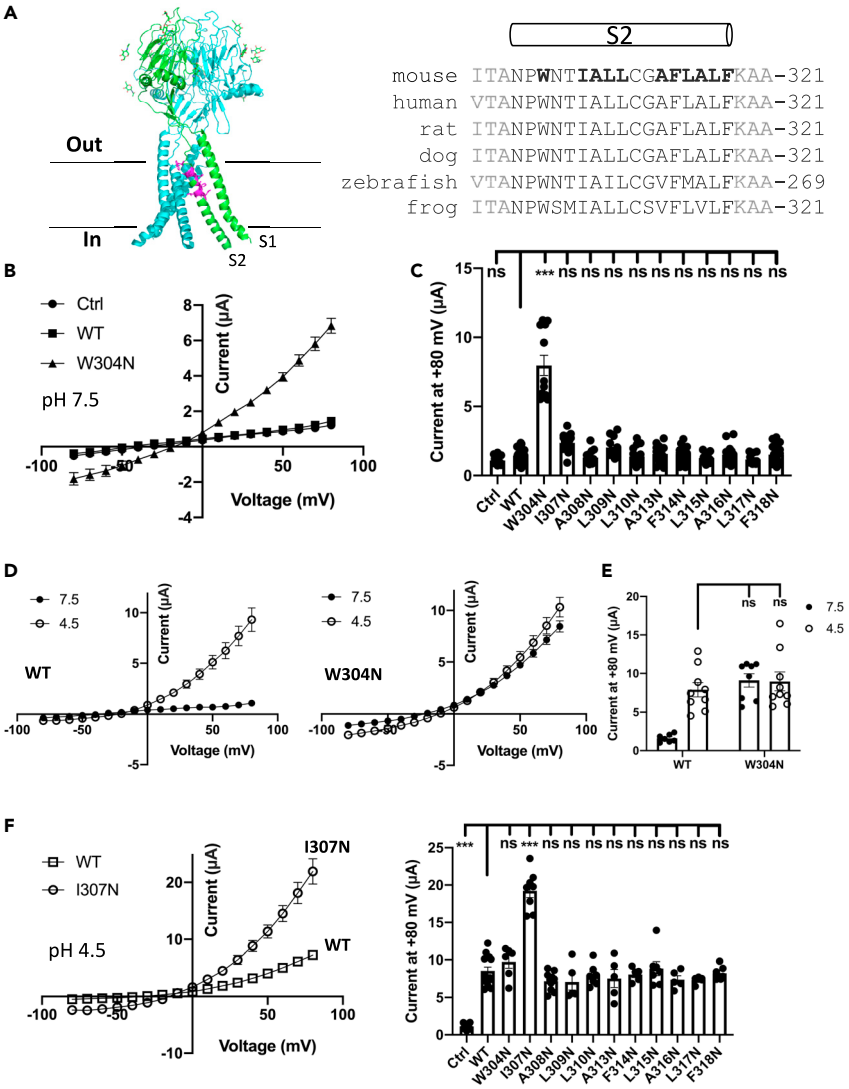

Figure 1. Effects of hydrophobic residues within helix S2 on the PAC function

(A) Left panel: structure of human PAC with hydrophobic candidate residues (W304, I307, A308, L309, L310, A313, F314, L315, A316, L317, F318 in magenta, PDB: 7JNA). Right panel: sequence alignment of the PAC S2 helix across species.

(B) Statistical I-V curves obtained from oocytes expressing WT PAC, mutant W304N, or from water-injected oocytes (Ctrl) bathed with the pH 7.5 solution (see STAR Methods).

(C) Bar charts of averaged currents at +80 mV from oocytes expressing WT or mutant PAC, as indicated. ***, $p < 0.001$; ns, not significant compared with WT PAC.

(D) Statistical I-V curves obtained from oocytes expressing WT PAC (left) or mutant W304N (right) at pH 7.5 (filled circle) or pH 4.5 (open circle).

(E) Averaged currents obtained from WT PAC or W304N expressing-oocytes at pH 7.5 or 4.5.

(F) Left panel: Statistical I-V curves corresponding to WT channel (open circle) or I307N (open square) at pH 4.5. Right panel: averaged currents for water-injected, WT PAC, or an indicated mutant at pH 4.5.

Data are represented as mean ± SEM. Also, see Figures S1 and S2.

not other nearby hydrophobic residues, is critical for maintaining PAC at closed states at pH 7.5. This is consistent with the fact revealed by the cryo-EM structure that W304 would face the ion permeation pathway at fenestrations.

We next examined the channel activity of the 11 mutants at extracellular pH 4.5 and found that mutant I307N exhibits much higher channel activity than that of WT PAC, while the other 10 mutants have similar

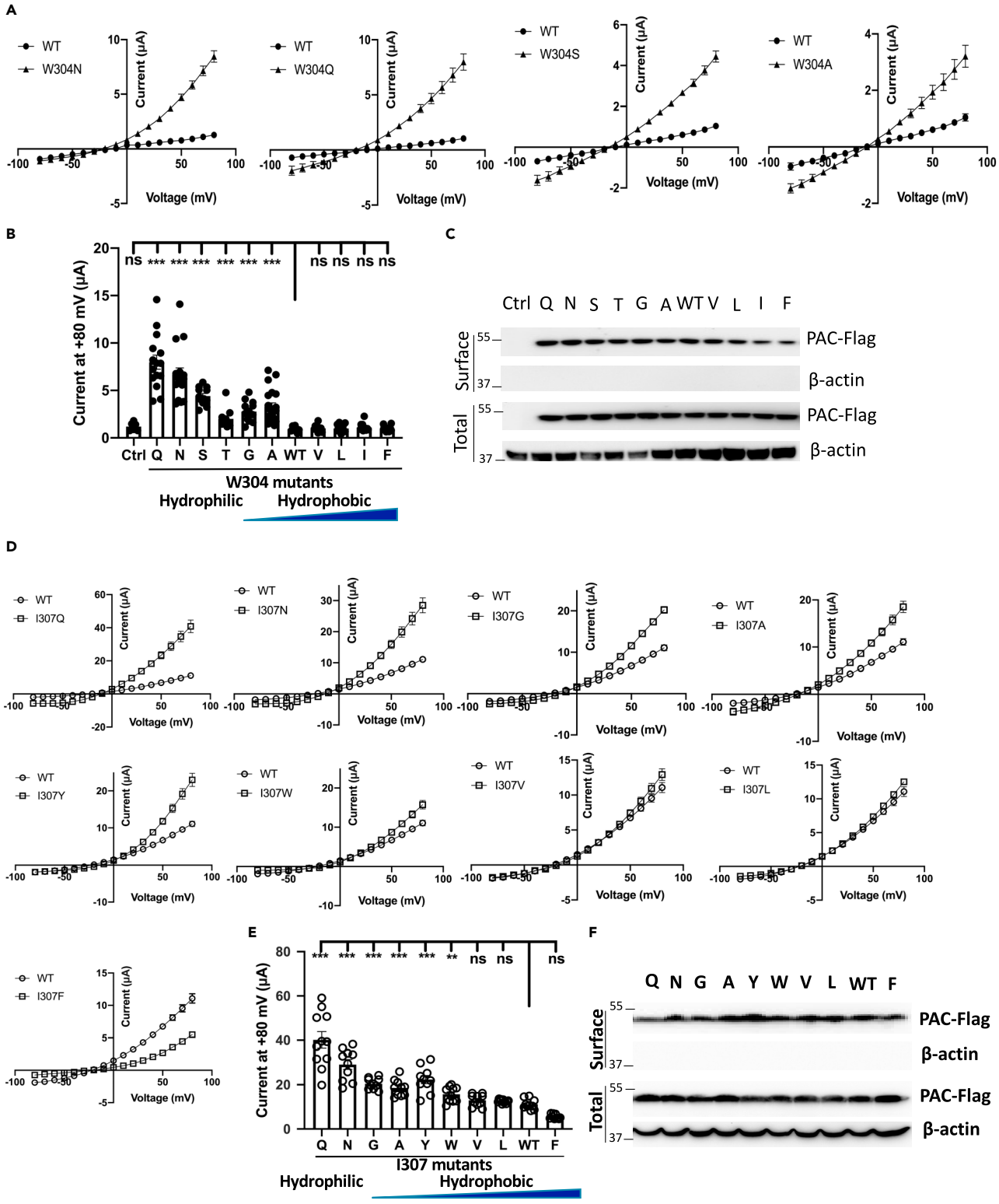

Figure 2. Effects of the hydrophobicity at sites 304 and 307 on the PAC function

(A) Statistical I-V curves obtained from oocytes expressing a W304 mutant at pH 7.5, in comparison with WT PAC.

(B) Averaged currents at +80 mV obtained from oocytes expressing WT PAC or a W304 mutant or water-injected oocytes at pH 7.5. ***, $p < 0.001$; ns, not significant compared with WT PAC.

Figure 2. *Continued*
(C) Total and surface expression of PAC-Flag or β-actin in oocytes similarly prepared as in panel (B).
(D) Statistical I-V curves from oocytes expressing an I307 mutant at pH 4.5, in comparison with WT channel in dashed lines.
(E) Averaged currents at +80 mV obtained from oocytes expressing WT or an I307 mutant at pH 4.5.
(F) Total and surface expression of PAC-Flag or β-actin in oocytes similarly prepared as in panel (E).
Data are represented as mean ± SEM. Also, see Figure S3.

activity as WT channel (Figure 1F). These data indicate that at the activated state (pH 4.5) the conserved hydrophobic residue I307 acts as an activation gate, while W304 functions as a "closed seal" at fenestrations at pH 7.5.

Correlation between the hydrophobicity at sites 304 and 307 and the channel function

To further understand the importance of gate hydrophobicity for the channel function we replaced W304 or I307 with different hydrophobic or hydrophilic residues. For the closed seal W304, mutation to hydrophilic Q, N, S, T, or less hydrophobic G or A constitutively opened the channel at pH 7.5, while mutation to other hydrophobic residues did not open the channel, after considering (normalizing by) their surface membrane expression determined with biotinylation (Figures 2A, 2B, 2C, and S3). Thus, the PAC activity at pH 7.5 inversely correlated with the hydrophobicity of site 304 (Figure 2B). Similarly, the PAC activity at pH 4.5 inversely correlated with the hydrophobicity of site 307 (Figures 2D, 2E, 2F, and S3). These data together strongly supported the concept that I307 acts as an activation gate within S2, while W304 acts as a closed seal at fenestrations.

We next investigated whether the W304 and I307 residues function independently. Hydrophilic mutation to Q or N was introduced simultaneously at W304 and I307. Different from single mutants at 304 or 307 (Figure 1), both double mutants W304Q/I307Q and W304N/I307N exhibited the constitutive open channel activity at pH 7.5 and significant activity increase upon extracellular acidification (Figure 3). Together, these data supported that W304 as a closed seal at fenestrations and I307 as an activation gate in S2 can independently exercise their roles at alkaline and acidic pH, respectively.

Identification and characterization of residues involved in proton binding sites

We reasoned that an amino acid residue involved in proton binding would be protonatable in acidic environments and thus would be either histidine (H), aspartic acid, or glutamic acid (Smith et al., 2007). As no known protein shares sequence homology to PAC (Yang et al., 2019), we performed sequence alignment across species and found 17 conserved protonatable residues located in the extracellular or cytosolic domain (Figure S4). We generated point mutants by neutralizing each of the 17 candidate residues (H to A, E to Q, and D to N) and found that mutants H131A, E224Q, D289N, and D297N, but not the other mutants, have significantly reduced proton-activated channel activity and proton affinity compared with the WT channel (Figures 4A, 4B, 4C, 4D, and S5). Furthermore, we found that the pH_{50} values for the four mutants significantly increase (Figure S6A), indicating the involvement of the four residues in proton binding. In addition, to test whether the two protonatable residues H98 and E107 may also be involved in proton binding, as suggested by the recently published structures (Ruan et al., 2020), we further found that the pH_{50} values of H98A and E107Q also significantly increase (Figure S6A). Taken together, we identified six protonatable residues in PAC that are presumably involved in proton binding (Figure S6B).

We next tested the function of a quadruple mutant with four residues neutralized (H131A/E224Q/D289N/D297N, briefed as AQNN) and found no significant channel activity at acidic pH 4.5 (Figures 4E and 4F), in support of the concept that these residues are important for proton binding. Interestingly, hydrophilic substitution at a fenestration site (W304N) constitutively opened the dead mutant channel AQNN even at pH 7.5 (Figures 4E–4G). This result indicates that while proton-induced PAC activation would require proton binding and the ensuing conformation changes, constitutive opening through hydrophilic substitution at a fenestration site (eg mutation W304N) does not seem to require proton binding or the resulting conformational changes. This suggests that while the PAC channel is constitutively opened via hydrophilic substitution at fenestration (W304) at pH 7.5 the rest of the channel protein would still be at a resting state rather than a (proton-induced) activated state.

Indication of constitutive channel activity of mutant W304N by its effect on cell death

Extracellular acidification was known to cause the death of cortical neuron and various cultured cells expressing PAC (Capurro et al., 2015; Ullrich et al., 2019; Yang et al., 2019). To further document the

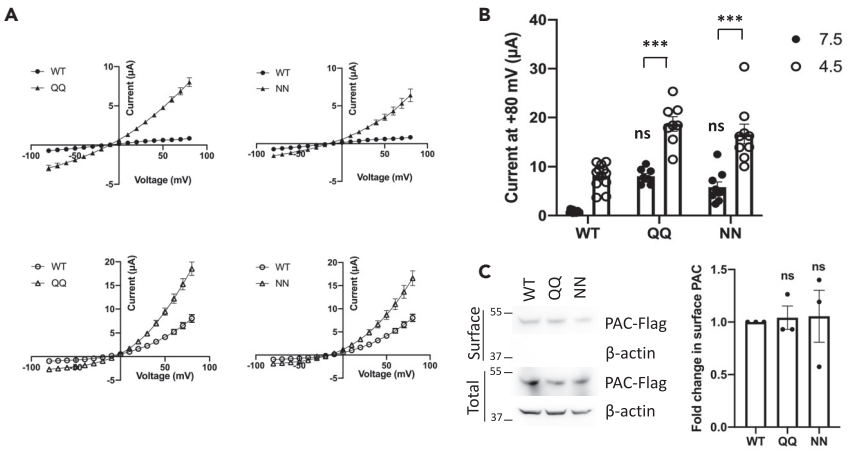

Figure 3. Functional effects of double hydrophilic mutations at W304 and I307

(A) Statistical I-V curves obtained from oocytes expressing WT, W304Q/I307Q, or W304N/I307N at pH 7.5 (filled) or 4.5 (open).

(B) Averaged currents at +80 mV obtained from oocytes expressing WT or a double mutant at pH 7.5 or 4.5. ***, $p < 0.001$; ns, not significant compared with the WT current at pH 4.5.

(C) Total and surface expression of PAC-Flag or β-actin in oocytes similarly prepared as in panel B (left panel) and statistical analysis (right panel). ns, not significant, compared with WT by Student's t-test.

Data are represented as mean ± SEM.

constitutive GOF nature of mutant W304N, we examined its effect on the acid-induced survival of cultured HEK293 and neuronal SH-SY5Y cells transfected with WT PAC or mutant W304N. Successful transfection of WT PAC and mutant W304N was confirmed by flow cytometry in both cell lines (Figures S7A–S7C). 48 h after transfection, incubation of HEK293 cells at 37°C for 2 h resulted in similar cell death at pH 7.5 and 4.5 when mutant W304N was expressed, in contrast to strong pH dependence of cell death when WT PAC was expressed (Figure 5). A similar toxic effect of mutant W304N at pH 7.5 was also observed in SH-SY5Y cells, a widely used *in vitro* neuronal cell model (Cai et al., 2015; Kovalevich and Langford, 2013) (Figure 6). Furthermore, Cl channel blocker 4,4′-diisothiocyano-2,2′-stilbenedisulfonic acid (DIDS) significantly reduced cell death (Figures 5 and 6), indicating that cell death is likely owing to PAC channel activity. Indeed, the presence of DIDS significantly inhibited the function of WT and mutant W304N channels (Figure S7D). Our data strongly supported the conclusion that mutant W304N is a GOF mutant at pH 7.5.

DISCUSSION

The ion flow in an ion channel may be controlled by single or multiple amino acid residues (Rao et al., 2018; Zheng et al., 2018c). The ion-conducting pathway and activation mechanism of the recently cloned PAC in living cells has remained largely unknown despite its structures resolved by means of cryo-EM (Deng et al., 2021; Ruan et al., 2020). Using *Xenopus* oocyte expression and the two-electrode electrophysiology, and based on the hydrophobic gate theory, we have identified and characterized two hydrophobic residues (W304 and I307) that are critical in controlling Cl flow in PAC and six protonatable residues (H98, E107, H131, E224, D289, and D297) that are implicated in proton-induced PAC activation. The GOF nature of PAC mutant W304N revealed by electrophysiology in oocytes has been verified based on its DIDS-inhibitable high toxicity in HEK293 and neuroblastoma SH-SY5Y cells.

At pH 7.5, reducing the hydrophobicity or size at fenestration site 304 was sufficient to potentiate the channel activity (Figure 2), while the hydrophobicity reduction at nearby hydrophobic sites (I307-L310 and A313-F318) had no effect (Figure 1). This fact indicates that none of the hydrophobic residues (I307-F318) proximal to the two pore constrictions functions as a pore gate at pH 7.5. Interestingly, a previous study using cysteine accessibility scanning identified I307 as a putative pore-lining residue but at acidic extracellular conditions (Ullrich et al., 2019; Yang et al., 2019). We thus examined the functional effects of hydrophilic substitutions at I307 and neighbor residues at pH 4.5 and found that only hydrophilic substitutions at site 307 results in further increases in the channel activity (Figure 1). Our data are consistent with the finding

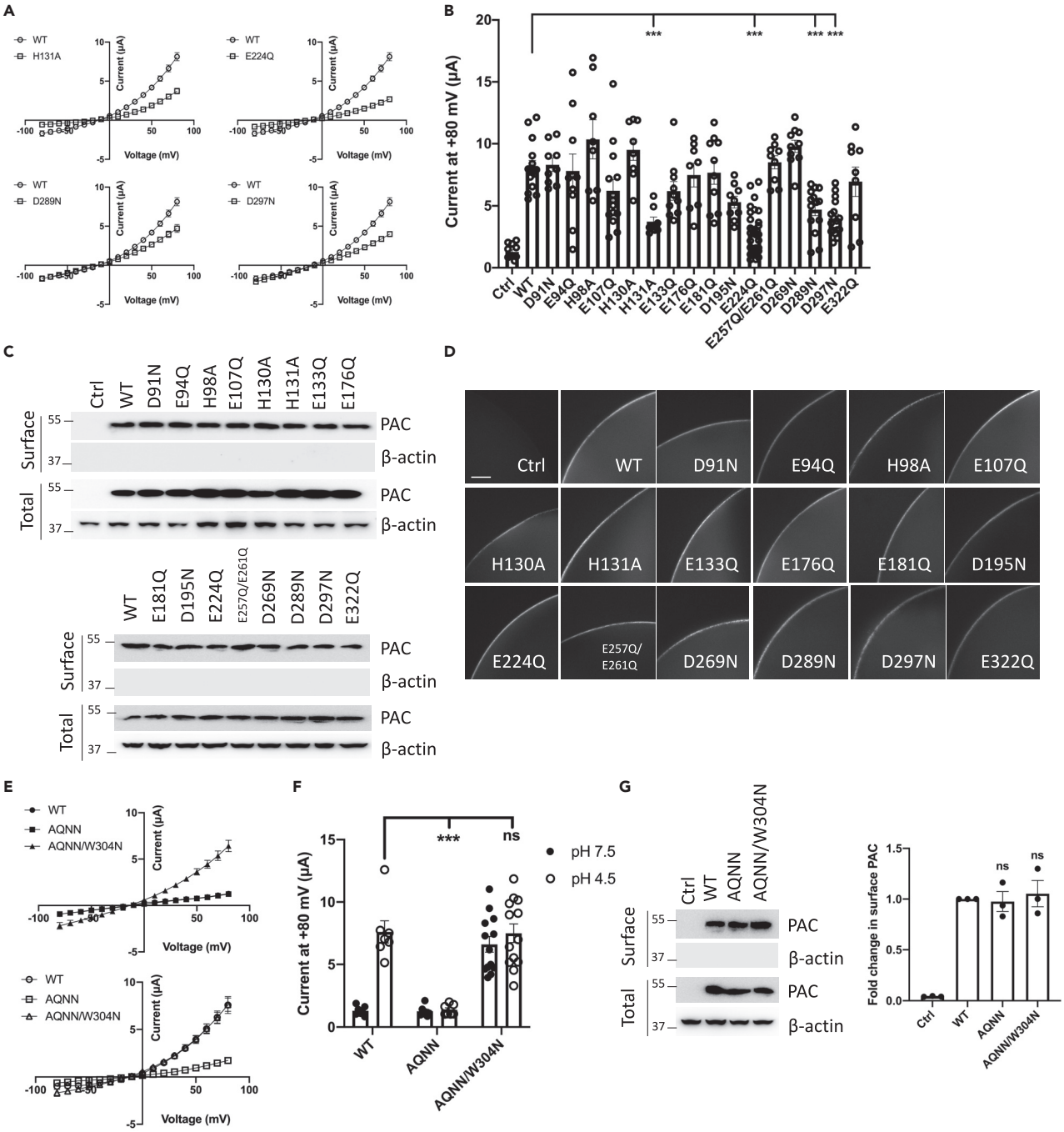

Figure 4. Functional effects of protonatable residues within the extracellular loop of PAC

(A) Statistical I-V curves obtained from oocytes expressing WT or mutant PAC at pH 4.5.

(B) Bar charts showing averaged currents for neutralized mutants, as indicated. ***, $p < 0.001$ by Student's t-test, in comparison with WT channel.

(C) Total and surface expression of PAC-Flag or β-actin in oocytes similarly prepared as in panel (B).

(D) Representative immunofluorescence images showing the surface expression of WT or mutant PAC.

(E) Statistical I-V curves obtained from oocytes expressing WT, mutant H131A/E224Q/D289N/D297N (AQNN) or W304N/AQNN at pH 7.5 (filled) or 4.5 (open). Scale bar, 50 μm.

(F) Averaged currents at +80 mV for indicated mutants.

(G) Total and surface expression of PAC-Flag or β-actin in oocytes similarly prepared as in panel F (left panel) and statistical analysis (right panel). ns, not significant, compared with WT by Student's t-test.

Data are represented as mean ± SEM. Also, see Figures S4–S6.

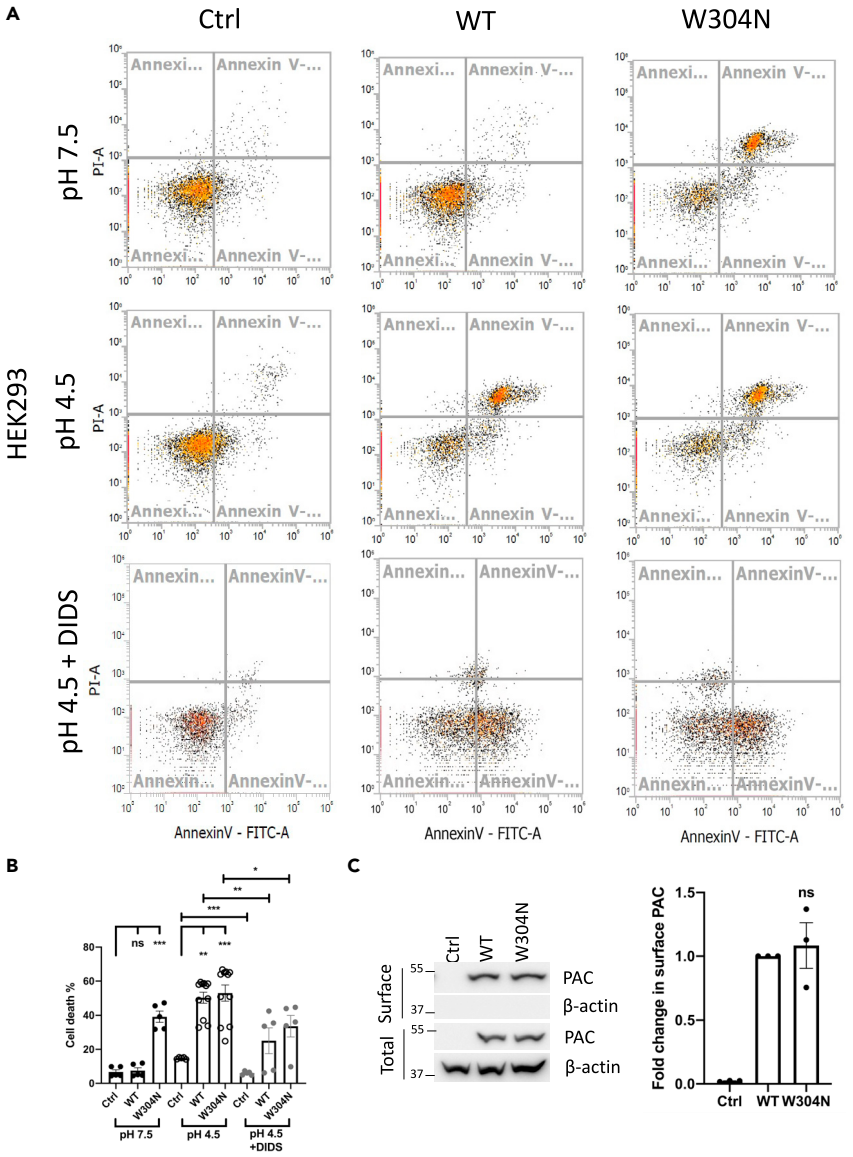

Figure 5. Effect of mutant W304N on the death of HEK293 cells

(A) Representative flow cytometry charts showing the FITC-Annexin/PI distribution of HEK293 cells transfected with plasmids encoding empty vector (Ctrl), WT PAC, or mutant W304N at pH 7.5 (upper), 4.5 (middle) or 4.5 + DIDS (100 μM) (lower).

(B) Averaged percentages of HEK293 cell death. ns, not significant; ***, $p < 0.001$; **, $p < 0.01$, by Student's t-test.

(C) Representative Western blot images showing the total or surface expression of PAC-Flag or β-actin in HEK293 cells. Data were averages obtained from three independent experiments.

Data are represented as mean ± SEM. Also, see Figure S7.

from the cysteine accessibility scanning (Ullrich et al., 2019; Yang et al., 2019) and for the first time indicate that I307 acts as an activation pore gate.

At pH 7.5, the hydrophobicity of site 307 did not affect the channel function, suggesting that I307 points away from the central pore, which is consistent with structures (Deng et al., 2021; Ruan et al., 2020). Similarly, the orientation of the fenestration residue W304 with respect to the ion flow pathway would also be pH-dependent, but in a reverse way. Thus, these data together suggest that the region that contains I307 and W304 may undergo twisting between alkalization and acidification. This mechanism of independent

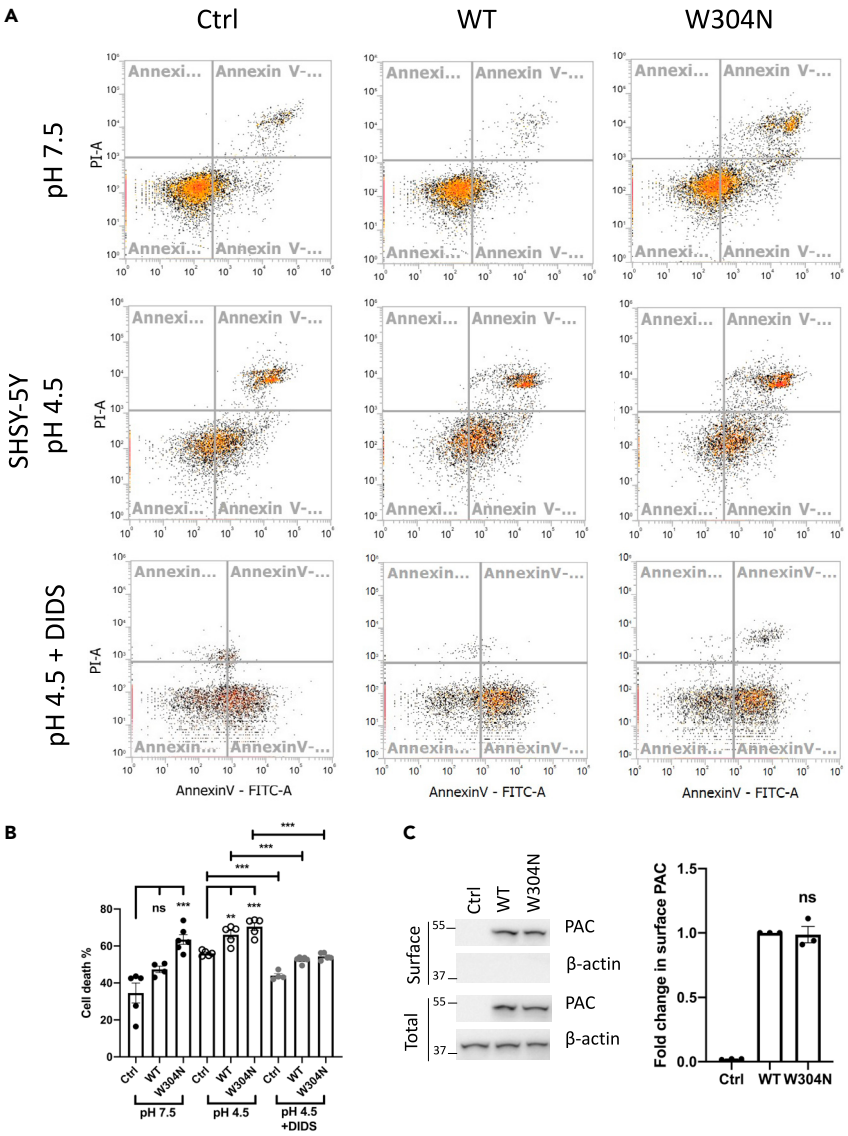

Figure 6. Effect of mutant W304N on the death of SH-SY5Y cells

(A) Representative flow cytometry charts showing the FITC-Annexin/PI distribution of SH-SY5Y cells transfected with plasmids encoding empty vector (Ctrl), WT PAC, or mutant W304N at pH 7.5 (upper), 4.5 (middle) or 4.5 + DIDS (100 μM) (lower).

(B) Averaged percentages of SH-SY5Y cell death. ns, not significant; ***, $p < 0.001$; **, $p < 0.01$, by Student's t-test.

(C) Representative Western blot images showing the total or surface expression of PAC-Flag or β-actin in SH-SY5Y cells.

Data were averages obtained from three independent experiments.

Data are represented as mean ± SEM. Also, see Figure S7.

controls by W304 at fenestrations and I307 within helix S2 for maintaining the closed and activated states, respectively, is somehow shared by other ion channels. For example, the trimeric mechano-sensitive channel Piezo1 possesses three fenestrations proposed to form ion permeation pathways (Zhao et al., 2018), whereas hydrophobic residues in an inner transmembrane helix are responsible for channel gating (Zheng et al., 2019).

The hydrophobic gate theory was originally proposed based on the observation of hydrating-dewetting transition in nanopore or nanotube by MD simulations (Aryal et al., 2015). Subsequent investigations extensively validated the theory in various ion channels, including but not limited to Cl channels, mechanically

activated channels, TRP channels, and potassium channels by means of electrophysiology, MD simulations, and structural studies (Aryal et al., 2015; Zheng et al., 2019). PAC activity displayed a strong inverse correlation with the hydrophobicity, but not with the residue size at site 307 at acidic pH. This is well supported by data obtained using hydrophilic and hydrophobic substitutions (Figure 2). At pH 4.5, substitution of I with larger but more hydrophilic Y and W increased the activity, while replacement with residues of similar hydrophobicity and various sizes (V, L, and F) did not significantly alter the function (Figure 2E). In summary, the hydrophobicity, but not the size, of gate residue I307 played a dominant role in regulating the PAC function, which seems to be shared by Ca-activated Cl channel bestrophin (Vaisey et al., 2016) but differs from the TRPP2 channel in which both the hydrophobicity and size of the gate residue L677 are important for the function (Zheng et al., 2018c).

The reported cryo-EM structures indicate that the pore constrictions are defined by several hydrophobic residues, including V100, M101, and V103 (forming upper constrictions) and L309 (pH 8), G312 (pH 8), and L315 (pH 8 and 4) (forming lower constrictions) (Deng et al., 2021; Ruan et al., 2020). However, hydrophilic N substitution at each of these six residues had no significant effect on PAC channel function at both pH 7.5 and 4.5 (Figures 1 and S8), indicating that they unlikely act as a functional gate residue in living cells. This is consistent with the finding that mutants V100A (Figure S8) and V100F (Deng et al., 2021), corresponding to V101F in Puffer Fish PAC, are GOF at both pH 7.5 and 4.5, indicating that V100 is functionally important but unlikely acts as a functional gate because substitution with a smaller (A) or bigger (F) hydrophobic residue both increased the channel function. Additionally, the valine residue defines a pore radius of less than 1 Å, too small to act as a functional gate to modulate Cl^- permeation. Consistently, MD simulations found permeability of Cl through the three lateral fenestrations but not the upper constriction (Ruan et al., 2020). Although cryo-EM structures revealed that L309 forms the narrowest path at pH 8 (Ruan et al., 2020) hydrophilic substituted mutants L309C and L309N had no function at pH 7.5 (Ullrich et al., 2019; Yang et al., 2019) and a similar function as WT PAC (Figure 1), respectively. It seems that in living cells L309 forms a lower physical constriction but does not constitute a functional pore gate. Moreover, the function of mutant channels G312C and L315C was not blocked by the MTSES application (Ullrich et al., 2019), suggesting that they do not face the pore. In addition to forming a closed seal, W304 is close (3.3 Å) to F83 located within S1 of a neighbor subunit (Deng et al., 2021; Ruan et al., 2020), which may form a π-π (F83:W304) interaction (Janiak, 2000). If an F83:W304 bonding indeed exits, the substitution of W304 with K (W304K) would retain a π-cation interaction (F83:K304) and mutant channel W304K would behave more or less like WT PAC. However, W304K was found to be a GOF mutant at pH 7.5 (Figure S8), which is consistent with other hydrophilic substitutions (Figure 2) that break the closed seal formed by W304 and increase the channel function (Figure 2). Mutant F83A, with disrupted π-π bonding, if exists, has a comparable function as WT PAC (Figure S9), which indicates that residue F83 and the F83:W304 bonding, if exists, are not functionally important. The inconsistencies between structural and functional data should presumably be due, at least in part, to different conditions between cryo-EM models and living cells, which give rise to different protein configurations. In addition, structures obtained from cryo-EM are a few static snapshots of PAC under non-physiological conditions, which contrasts with the dynamic gating processes of PAC in living cells.

Activated PAC was previously predicted to bind three to four protons based on a Hill coefficient of 3.6 (Lambert and Oberwinkler, 2005). Neutralization of residues involved in the proton binding decreases the corresponding Hill coefficients compared with WT (Figure S6A), which indicates the proton binding in each mutant is impaired. The involvement of four out of the six residues, H98, E107, E224, and D289 (latter two corresponding to E226 and D290 in pufferfish PAC, respectively) in proton binding was supported by recent structural studies (Deng et al., 2021; Ruan et al., 2020). Although normal physiological conditions correspond to a pH range of 7.2–7.4 extracellular pH can be as low as 5.5 in inflammatory reactions, 5.7 outside tumors, and 6.5 during stroke (Rehncrona, 1985; Tong et al., 2011). Furthermore, as the pH_{50} value at 37°C may rise to around 6.0 (Yang et al., 2019), it is possible that PAC plays role in inflammation, carcinogenesis, or ischemia-reperfusion injury in vivo. Our identification and characterization of GOF and acid-insensitive mutants would help understand the physiological roles of PAC, for example, through studies utilizing mutant knock-in animals.

Limitations of the study

This study proposed a mechanism on how distinct hydrophobic residues W304 and I307 affect the PAC channel activity and characterized putative proton sensing amino acid residues in the extracellular region.

Although cryo-EM structures and our functional experiments supported the concept that W304 would face the ion permeation pathway at fenestrations, we recognized that an additional independent experiment, for example, using a membrane impermeant thiol modifying reagent to mutant W304C would further verify the concept. Regarding mutant AQNN, which was a loss-of-function as shown by electrophysiology and biotinylation, its role in acid-induced cell death of cultured mammalian cells has not been tested in this study although we expected that AQNN-expressing cells would resemble the control cells.

STAR★METHODS

Detailed methods are provided in the online version of this paper and include the following:

- KEY RESOURCES TABLE
- RESOURCE AVAILABILITY
  - Lead contact
  - Materials availability
  - Data and code availability
- EXPERIMENTAL MODEL AND SUBJECT DETAILS
  - Plasmids, mutagenesis, antibodies, chemicals and cell lines
  - Expression in *Xenopus* oocytes
  - Two-electrode voltage clamp electrophysiology
  - Immunostaining
  - Cell culture and transfection
  - Acid-induced cell death and flow cytometry
  - Immunoblotting and biotinylation
- QUANTIFICATION AND STATISTICAL ANALYSIS

SUPPLEMENTAL INFORMATION

Supplemental information can be found online at https://doi.org/10.1016/j.isci.2021.103395.

ACKNOWLEDGMENTS

We would like to thank Vanessa Vuong for helping in experiments. This work was supported by the Natural Sciences and Engineering Research Council of Canada (NSERC) (to X.Z.C.) and National Natural Science Foundation of China (grant # 31871176 and 32070726, to J.T). R.C. was a recipient of the Dean's Doctoral Awards, Alberta Innovates Graduate Student Scholarship and NSERC International Research Training Group Studentship.

AUTHOR CONTRIBUTIONS

Conceptualization, R.C. and X.-Z.C.; Investigation, R.C. Supervision, J.T. and X.-Z.C. Writing, R.C. and X.-Z.C.

DECLARATION OF INTERESTS

The authors declare no competing financial interests.

Received: July 30, 2020
Revised: July 13, 2021
Accepted: October 28, 2021
Published: December 17, 2021

REFERENCES

Aryal, P., Sansom, M.S., and Tucker, S.J. (2015). Hydrophobic gating in ion channels. J. Mol. Biol. *427*, 121–130.

Auzanneau, C., Thoreau, V., Kitzis, A., and Becq, F. (2003). A Novel voltage-dependent chloride current activated by extracellular acidic pH in cultured rat Sertoli cells. J. Biol. Chem. *278*, 19230–19236.

Cai, R., Xue, W., Liu, S., Petersen, R.B., Huang, K., and Zheng, L. (2015). Overexpression of glyceraldehyde 3-phosphate dehydrogenase prevents neurovascular degeneration after retinal injury. FASEB J. *29*, 2749–2758.

Capurro, V., Gianotti, A., Caci, E., Ravazzolo, R., Galietta, L.J., and Zegarra-Moran, O. (2015). Functional analysis of acid-activated Cl(-) channels: properties and mechanisms of regulation. Biochim. Biophys. Acta *1848*, 105–114.

Deng, Z., Zhao, Y., Feng, J., Zhang, J., Zhao, H., Rau, M.J., Fitzpatrick, J.A.J., Hu, H., and Yuan, P. (2021). Cryo-EM structure of a proton-activated chloride channel TMEM206. Sci. Adv. *7*, eabe5983.

Dong, K., Yao, N., Pu, Y., He, X., Zhao, Q., Luan, Y., Guan, W., Rao, S., and Ma, Y. (2014). Genomic scan reveals loci under altitude adaptation in Tibetan and Dahe pigs. PLoS One *9*, e110520.

Duran, C., Thompson, C.H., Xiao, Q., and Hartzell, H.C. (2010). Chloride channels: often enigmatic, rarely predictable. Annu. Rev. Physiol. *72*, 95–121.

Janiak, C. (2000). A critical account on pi-pi stacking in metal complexes with aromatic nitrogen-containing ligands. J. Chem. Soc. Dalton *2000*, 3885–3896.

Kovalevich, J., and Langford, D. (2013). Considerations for the use of SH-SY5Y neuroblastoma cells in neurobiology. Methods Mol. Biol. *1078*, 9–21.

Lambert, S., and Oberwinkler, J. (2005). Characterization of a proton-activated, outwardly rectifying anion channel. J. Physiol. *567*, 191–213.

Lardner, A. (2001). The effects of extracellular pH on immune function. J. Leukoc. Biol. *69*, 522–530.

Ma, Z.Y., Zhang, W., Chen, L., Wang, R., Kan, X.H., Sun, G.Z., Liu, C.X., Li, L., and Zhang, Y. (2008). A proton-activated, outwardly rectifying chloride channel in human umbilical vein endothelial cells. Biochem. Biophys. Res. Commun. *371*, 437–440.

Planells-Cases, R., and Jentsch, T.J. (2009). Chloride channelopathies. Biochim. Biophys. Acta *1792*, 173–189.

Rao, S., Lynch, C.I., Klesse, G., Oakley, G.E., Stansfeld, P.J., Tucker, S.J., and Sansom, M.S.P. (2018). Water and hydrophobic gates in ion channels and nanopores. Faraday Discuss. *209*, 231–247.

Rehncrona, S. (1985). Brain acidosis. Ann. Emerg. Med. *14*, 770–776.

Ruan, Z., Osei-Owusu, J., Du, J., Qiu, Z., and Lu, W. (2020). Structures and pH-sensing mechanism of the proton-activated chloride channel. Nature *588*, 350–354.

Sato-Numata, K., Numata, T., and Okada, Y. (2014). Temperature sensitivity of acid-sensitive outwardly rectifying (ASOR) anion channels in cortical neurons is involved in hypothermic neuroprotection against acidotoxic necrosis. Channels (Austin) *8*, 278–283.

Smith, E.S., Zhang, X., Cadiou, H., and McNaughton, P.A. (2007). Proton binding sites involved in the activation of acid-sensing ion channel ASIC2a. Neurosci. Lett. *426*, 12–17.

Terry, J. (1994). The major electrolytes: sodium, potassium, and chloride. J. Intraven. Nurs. *17*, 240–247.

Tong, J., Wu, W.N., Kong, X., Wu, P.F., Tian, L., Du, W., Fang, M., Zheng, F., Chen, J.G., Tan, Z., et al. (2011). Acid-sensing ion channels contribute to the effect of acidosis on the function of dendritic cells. J. Immunol. *186*, 3686–3692.

Ullrich, F., Blin, S., Lazarow, K., Daubitz, T., von Kries, J.P., and Jentsch, T.J. (2019). Identification of TMEM206 proteins as pore of PAORAC/ASOR acid-sensitive chloride channels. Elife *8*, e49187.

Vaisey, G., Miller, A.N., and Long, S.B. (2016). Distinct regions that control ion selectivity and calcium-dependent activation in the bestrophin ion channel. Proc. Natl. Acad. Sci. U S A *113*, E7399–E7408.

Valinsky, W.C., Touyz, R.M., and Shrier, A. (2017). Characterization of constitutive and acid-induced outwardly rectifying chloride currents in immortalized mouse distal tubular cells. Biochim. Biophys. Acta Gen. Subj. *1861*, 2007–2019.

Wang, H.Y., Shimizu, T., Numata, T., and Okada, Y. (2007). Role of acid-sensitive outwardly rectifying anion channels in acidosis-induced cell death in human epithelial cells. Pflugers Arch. *454*, 223–233.

Yamamoto, S., and Ehara, T. (2006). Acidic extracellular pH-activated outwardly rectifying chloride current in mammalian cardiac myocytes. Am. J. Physiol. Heart Circ. Physiol. *290*, H1905–H1914.

Yang, J., Chen, J., Del Carmen Vitery, M., Osei-Owusu, J., Chu, J., Yu, H., Sun, S., and Qiu, Z. (2019). PAC, an evolutionarily conserved membrane protein, is a proton-activated chloride channel. Science *364*, 395–399.

Yi, X., Liang, Y., Huerta-Sanchez, E., Jin, X., Cuo, Z.X., Pool, J.E., Xu, X., Jiang, H., Vinckenbosch, N., Korneliussen, T.S., et al. (2010). Sequencing of 50 human exomes reveals adaptation to high altitude. Science *329*, 75–78.

Zhao, Q., Zhou, H., Chi, S., Wang, Y., Wang, J., Geng, J., Wu, K., Liu, W., Zhang, T., Dong, M.Q., et al. (2018). Structure and mechanogating mechanism of the Piezo1 channel. Nature *554*, 487–492.

Zheng, W., Cai, R., Hofmann, L., Nesin, V., Hu, Q., Long, W., Fatehi, M., Liu, X., Hussein, S., Kong, T., et al. (2018a). Direct binding between pre-S1 and TRP-like domains in TRPP channels mediates gating and functional regulation by PIP2. Cell Rep. *22*, 1560–1573.

Zheng, W., Gracheva, E.O., and Bagriantsev, S.N. (2019). A hydrophobic gate in the inner pore helix is the major determinant of inactivation in mechanosensitive Piezo channels. Elife *8*, e44003.

Zheng, W., Hu, R., Cai, R., Hofmann, L., Hu, Q., Fatehi, M., Long, W., Kong, T., Tang, J., Light, P., et al. (2018b). Identification and characterization of hydrophobic gate residues in TRP channels. FASEB J. *32*, 639–653.

Zheng, W., Yang, X., Hu, R., Cai, R., Hofmann, L., Wang, Z., Hu, Q., Liu, X., Bulkley, D., Yu, Y., et al. (2018c). Hydrophobic pore gates regulate ion permeation in polycystic kidney disease 2 and 2L1 channels. Nat. Commun. *9*, 2302.

STAR★METHODS

KEY RESOURCES TABLE

REAGENT or RESOURCE	SOURCE	IDENTIFIER
Antibodies		
FLAG Tag (D6W5B) rabbit mAb	Cell Signaling Technology	Cat# 14793; RRID:AB_2800094
Myc tag	Cell Signaling Technology	Cat# 2276S; RRID:AB_331783
β-actin	Santa Cruz Biotechnology	Cat# sc-47778; RRID:AB_2714189
Alexa fluor 488 conjugated Myc-tag	Cell Signaling Technology	Cat# 2279S; RRID:AB_2151849
Bacterial and virus strains		
Subcloning Efficiency™ DH5α competent cells	Invitrogen	Cat# 18265017
Chemicals, peptides, and recombinant proteins		
4,4′-diisothiocyano-2,2′-stilbenedisulfonic acid	Tocris	Cat# 4523
Critical commercial assays		
mMESSAGE mMACHINE T7 transcription kit	Invitrogen	Cat# AM1344
Q5 site-directed mutagenesis kit	New England Biolabs	Cat# E0554S
eBioscience annexin V-FITC apoptosis detection kit	Invitrogen	Cat# BMS500FI-20
Experimental models: Cell lines		
HEK293	ATCC	CRL-1573
SH-SY5Y	ATCC	CRL-2266
Experimental models: Organisms/strains		
Xenopus laevis	National Xenopus Resource	Wild-Type Frogs *X. laevis* NXR_0031
Oligonucleotides		
Primers used in this study, see Table S1	Integrated DNA Technologies	NA
Recombinant DNA		
pCMV-PACC1-flag/Myc	OriGene Technologies	Cat# : MR205311
Software and algorithms		
Prism 8	GraphPad	https://www.graphpad.com/scientific-software/prism/
pClamp 9	Axon Instruments	https://support.moleculardevices.com/s/article/Axon-pCLAMP-9-Electrophysiology-Data-Acquisition-Analysis-Software-Download-Page
Volocity	Quorum Technologies	https://quorumtechnologies.com/index.php/component/content/category/31-volocity-software

RESOURCE AVAILABILITY

Lead contact

Further requests should be directed to and will be fulfilled by the lead contact Dr. Xing-Zhen Chen (xzchen@ualberta.ca).

Materials availability

Materials are available upon reasonable request.

Data and code availability

- No dataset was generated from or used in this study.
- No original code was reported in this study.
- Additional information related to this study will be fulfilled by the lead contact upon request.

EXPERIMENTAL MODEL AND SUBJECT DETAILS

Plasmids, mutagenesis, antibodies, chemicals and cell lines

Plasmid encoding mouse PAC (GenBank: NM_025864) with Flag and Myc tags in the pCMV vector was purchased from OriGene (Rockville, MD). Mutations were introduced using Q5 site-directed mutagenesis kit (New England Biolabs, Ipswich, MA) and confirmed by sequencing. Primers were synthesized by Integrated DNA Technologies (Coralville, IA) and listed in Table S1. Flag, Myc, β-actin and Alexa Fluor 488 conjugated Myc-tag antibodies were from Cell Signaling Technology (Danvers, MA) or Santa Cruz Biotechnology (Dallas, TX). Anti-rabbit and anti-mouse secondary antibodies were from GE Healthcare (Waukesha, WI). DIDS was purchased from Tocris (Bristol, United Kingdom). Human neuroblastoma cell line SH-SY5Y was a gift of Dr. Thomas Simmen (University of Alberta, Edmonton, Canada).

Expression in *Xenopus* oocytes

mMESSAGE mMACHINE T7 transcription kit (Invitrogen, Waltham, MA) was used to generate capped RNAs encoding WT and mutant PAC. 25 ng cRNA was injected into each oocyte with a microinjection dispense system Picospritzer III (Parker Hannifin, Hollis, NH) (Zheng et al., 2018a). Water-injected oocytes were served as control. Injected oocytes were cultured at 18°C for 2–3 days prior to experiments. The present study was approved by the Ethical Committee for Animal Experiments of the University of Alberta and carried out in accordance with the Guidelines for Research with Experimental Animals of the University of Alberta and the Guide for the Care and Use of Laboratory Animals (NIH) revised in 1996.

Two-electrode voltage clamp electrophysiology

Two capillary pipettes (Warner Instruments, Hamden, CT) with a tip resistance of 0.3–2 MΩ and filled with 3 M KCl were used to penetrate an oocyte. Oocyte whole-cell currents were recorded at RT and perfused with extracellular solutions described in figure legends. Currents and voltages were digitized at 200 μs/sample and Bessel filtered at 2 kHz, with a GeneClamp 500B Amplifier and Digidata 1322A AD/DA converter (Molecular Devices, Union City, CA). I-V curves were obtained by application of a ramp protocol with voltages from - 100 mV to +100 mV during 1 s. Oocytes were bathed in a pH 7.5 (or 4.5) solution composed of (in mM) 100 NaCl, 2 KCl, 1 $MgCl_2$ and 10 HEPES with pH adjusted by NaOH (or 5 Na_3-citrate with pH adjusted by citrate acid). Resulting data were analyzed with pClamp 9 (Axon Instruments, Union City, CA) and plotted with GraphPad Prism 8 (GraphPad Software, San Diego, CA).

Immunostaining

Whole mount oocytes were washed with PBS and fixed with 4% paraformaldehyde at RT for 15 min. After permeabilization with 0.1% Triton for 5 min, oocytes were incubated with 3% skim milk for 30 min. Diluted Flag antibody was used to incubate oocytes at 4°C overnight, which were next incubated with secondary anti-mouse IgG Fab2 Alexa Fluor 555 (Cell Signaling Technology) for 1 h at RT. Oocytes were mounted with Fisher Chemical Permount mounting medium (Fisher Scientific) and examined with an Olympus IX-81 spinning confocal microscope (Cell Imaging Center, Faculty of Medicine and Dentistry, University of Alberta). Mammalian cells for immunostaining underwent a similar procedure but were mounted with ProLong Gold Antifade Mountant (Molecular Probes, Life Technologies).

Cell culture and transfection

HEK293 and SH-SY5Y cells were maintained in Dulbecco's modified Eagle's medium with 1% penicillin/streptomycin and 10% FBS (Gibco) in an incubator with 5% CO_2. Transient expression of WT or mutant PAC was performed following the FUGENE HD Transfection Reagent manual (Promega, WI).

Acid-induced cell death and flow cytometry

Transfected HEK293 or SH-SY5Y cells were incubated with an acidic or alkaline buffer, composed of (in mM) 145 NaCl, 2 KCl, 2 $MgCl_2$, 1.5 $CaCl_2$, 10 glucose, and 10 HEPES (for the alkaline buffer at pH 7.5, adjusted with NaOH) or 5 Na_3-citrate (for the acidic buffer at pH 4.5, adjusted with citric acid), for 2 h at 37°C. Cells were collected for flow cytometry analysis with eBioscience Annexin V-FITC Apoptosis Detection Kit (Thermo Fisher Scientific, Waltham, MA), using Attune NxT cytometer in the Flow Cytometry Facility (Faculty of Medicine and Dentistry, University of Alberta). Cell death percentage equals to $[1- \frac{n\ (Annexin\ V-FITC^-/PI^-\ cells)}{n\ (total\ cell)}] \times 100$. Dead (non-viable) cells included Annexin V-FITC$^-$/PI$^+$, Annexin V-FITC$^+$/PI$^-$ and Annexin V-FITC$^+$/PI$^+$ cells. To evaluate transfection efficiency, cells were immunostained

with Alexa Fluor 488 conjugated Myc-tag antibody following manufacture's guide and examined by flow cytometry.

Immunoblotting and biotinylation

For the total protein expression, oocytes or mammalian cells were lysed using CelLytic MT Cell Lysis Reagent (Sigma, Oakville, ON). Lysates were subjected to SDS-PAGE and immunoblotted using the corresponding antibodies. For the surface expression, oocytes or mammalian cells were bathed with pre-cooled PBS solution and then treated with EZ-Link Sulfo-NHS-SS-Biotin (Pierce, Rockford, IL) at RT. After quenching the extra biotin and washing cells were lysed for Western blot examination.

QUANTIFICATION AND STATISTICAL ANALYSIS

All data were presented as mean ± SEM (standard error of the mean). p values of less than 0.05, 0.01 and 0.001, were assigned with *, ** and ***, respectively and were calculated by Student's t-test. Statistically not significant was abbreviated as 'ns'.